

# Role of Acidic Pretreatment of Layered Silicate RUB-15 in Its Topotactic Conversion into Pure Silica Sodalite

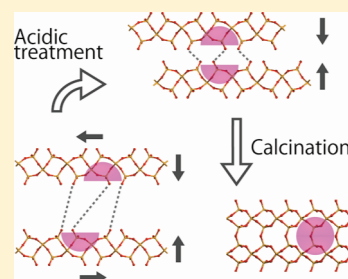
Takahiko Moteki,<sup>†</sup> Watcharop Chaikittisilp,<sup>†,§</sup> Yasuhiro Sakamoto,<sup>‡</sup> Atsushi Shimojima,<sup>†</sup> and Tatsuya Okubo<sup>\*,†</sup>

<sup>†</sup>Department of Chemical System Engineering, The University of Tokyo, Bunkyo-ku, Tokyo, 113-8656 Japan

<sup>‡</sup>Nanoscience and Nanotechnology Research Center, Osaka Prefecture University, Sakai, 599-8570 Japan

 Supporting Information

**ABSTRACT:** Topotactic conversion of crystalline layered silicates into zeolite provides an opportunity to create new chemical compositions, framework types, and macroscopic morphologies that are difficult to achieve by conventional hydrothermal synthesis. We have recently reported the successful synthesis of pure silica sodalite with a unique sheet-like morphology from layered silicate RUB-15 occluding interlayer TMA<sup>+</sup> cations. Pretreatment of RUB-15 with acetic acid was found to be crucial for topotactic dehydration–condensation between the silicate layers upon heating. In this study, a homologous series of carboxylic acids of varying concentrations is examined for their capability to generate an ordered intermediate state, and important factors for topotactic conversion are determined. Both length of the alkyl chains and concentration of the carboxylic acids strongly affected the crystallinity of the products, and well-crystallized sodalite was obtained using either acetic or propionic acid. Transmission electron microscopy showed that the sodalite with sheet-like morphology has the thickness of several hundred nanometers in which the (110) plane is oriented parallel to the surface. Two key factors elucidated for successful conversion are (i) proton-exchange of interlayer TMA<sup>+</sup> cations to shorten the interlayer distance and to form Si–OH groups and (ii) intercalation of carboxylic acid molecules between the layers to maintain the well-ordered layered structure prior to calcination.



**KEYWORDS:** zeolites, layered silicates, porous materials, topotactic conversion, silica

## INTRODUCTION

Microporous crystalline materials such as zeolites and metal–organic frameworks (MOFs) are potentially useful as catalysts, adsorbents, and separation membranes.<sup>1</sup> Zeolite frameworks, which are constructed from TO<sub>4</sub> tetrahedral units (T = Si, Al, P, Ge, Ga, etc.), are currently classified into more than 190 types by the International Zeolite Association (IZA).<sup>2</sup> Designed synthesis of new zeolites with unique pore geometries would drive the zeolite community toward on-demand applications. Historically, although most of the new zeolites were synthesized in the presence of organic structure-directing agents (SDAs), only a few molecules exhibited real structure-directing function.<sup>3,4</sup> In fact, syntheses of zeolite and zeotype materials have been carried out by “black-box” hydrothermal reactions; thus, trial-and-error is still a routine practice for discovering new structures, although the approach becomes more strategic and systematic than before. On the other hand, MOFs are modularly synthesized by self-assembly of transition-metal clusters as nodes and organic molecules as struts, leading to tunable frameworks and function.<sup>1b,5</sup> Such features make them attractive for emerging applications such as hydrogen storage and enantioselective catalysis.<sup>6</sup>

Such a bottom-up concept has also been applied to the synthesis of zeolites from layered silicates, considered as two-dimensional building blocks, by topotactic conversion into three-dimensional frameworks.<sup>7</sup> In this conversion, zeolite is formed by dehydration–condensation of two facing silanol groups on the

neighboring layers ( $\equiv\text{Si}-\text{OH} + \text{HO}-\text{Si}\equiv \rightarrow \equiv\text{Si}-\text{O}-\text{Si}\equiv + \text{H}_2\text{O}$ ) upon thermal calcination; thus, the resultant zeolite reflects the framework of the original layered silicate. This approach enables the synthesis of zeolites with unique frameworks and new chemical compositions that are not yet accessible by conventional hydrothermal reactions. Successful topotactic conversion of layered silicates into zeolites requires several structural and chemical complements such as the positions of the silanol groups or the interlayer distances. Thus far, zeolites MWW, ferrierite, CDS-1, Nu-6(2), EU-20b, RUB-24, RUB-41, and sodalite have been constructed from layered silicates ERB-1, PREFER, PLS-1, Nu-6(1), EU-19, RUB-18, RUB-39, and RUB-15, respectively.<sup>7</sup> Among the aforementioned zeolites, only MWW, ferrierite, and sodalite structures can be obtained both by direct hydrothermal synthesis and by topotactic conversion with the help of organic SDAs.

Recently, we reported a new route to synthesize pure silica sodalite by topotactic conversion of layered silicate RUB-15 ( $[\text{N}(\text{CH}_3)_4]_8[\text{Si}_{24}\text{O}_{52}(\text{OH})_4] \cdot 20\text{H}_2\text{O}$ ).<sup>7h,8</sup> The resulting silica sodalite possesses sheet-like morphology and hollow sodalite cages. This unique morphology provides an opportunity for novel uses of sodalite, in particular, as separation membranes and sensors. In conventional hydro- and solvothermal syntheses, silica

Received: May 25, 2011

Revised: June 28, 2011

Published: July 13, 2011

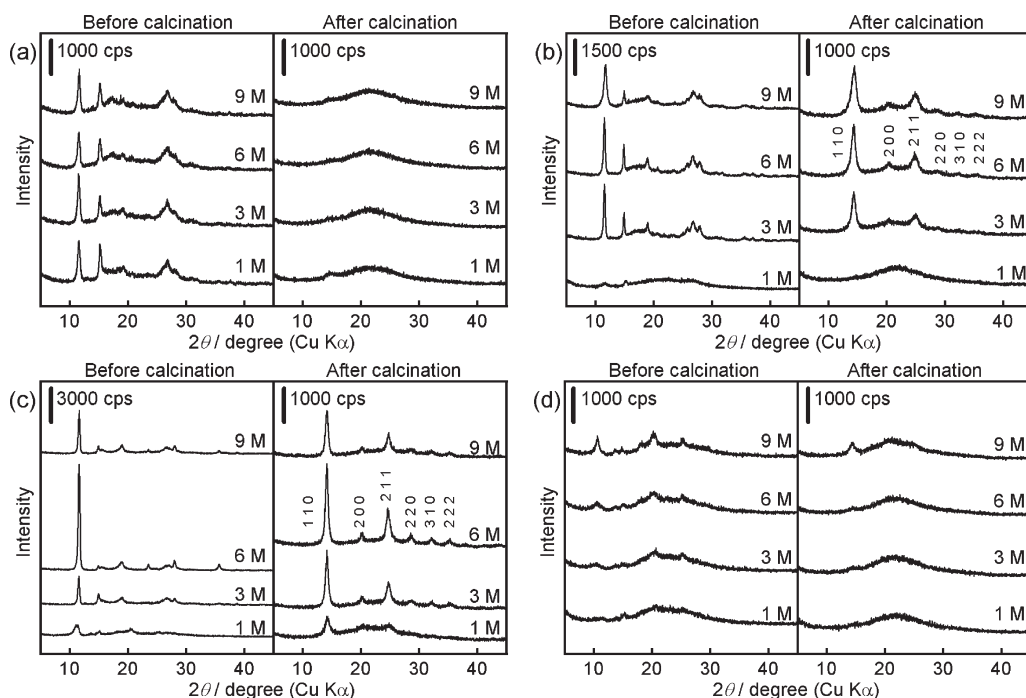


**Figure 1.** XRD patterns of RUB-15 samples treated with (a) formic acid, (b) acetic acid, (c) propionic acid, and (d) butyric acid at various concentrations (left) and their corresponding calcined products (right). All of the acidic pretreatments were carried out for 3 h.

sodalite is typically formed with occluded organic SDAs or solvent that is difficult to remove without structural collapse. As a result, the ultrasmall micropores of silica sodalite cannot be used effectively because of such guest inclusion. The novel silica sodalite synthesized by topotactic conversion exhibits accessible micropores, which allow very tiny molecules such as hydrogen to pass through.

To obtain well-crystallized sodalite, pretreatment of RUB-15 with acetic acid prior to calcination was considered to be a crucial step because only amorphous products were obtained from untreated or HCl-treated RUB-15 under our experimental conditions.<sup>7h</sup> This result is in contrast to that observed for another zeolite, RUB-24, which can be formed from both acetic acid- and HCl-treated layered silicate RUB-18.<sup>9</sup> Upon pretreatment of RUB-15 with acetic acid, TMA<sup>+</sup> cations are exchanged with protons thereby shortening the interlayer distance. In addition, intercalation of acetic acid between the silicate layers was also suggested.<sup>7h</sup> Such changes in the interlayer environment are expected to affect the subsequent condensation process and the final structure. A deeper understanding of the role of the requisite carboxylic acid would lead to further development of zeolite syntheses by topotactic conversion.

Herein, we discuss the variable effects of a homologous series of carboxylic acids ( $C_nH_{2n+1}COOH$ , where  $n = 0-3$ ) on the formation of pure silica sodalite. Only acetic and propionic acids ( $n = 1$  and  $2$ , respectively) can be well intercalated into the interlayer space and thereby result in the well-crystallized sodalite. Interestingly, in some conditions, acidic pretreatment of RUB-15 for a time frame as short as 10 s is sufficient for the formation of highly crystalline silica sodalite.

## EXPERIMENTAL SECTION

**Synthesis of RUB-15.** RUB-15 was synthesized by a hydrothermal treatment of hydrated crystalline double four-membered ring (D4R)

silicate ammonium salt prepared according to previous reports.<sup>7h,14</sup> In a typical synthesis, tetraethoxysilane (TEOS, Tokyo Kasei Kogyo Co. Ltd.) was added to tetramethylammonium hydroxide (TMAOH, 25 wt % in water, Wako Pure Chemical Industry) at a TEOS/TMAOH molar ratio of 1. The concentration of Si was adjusted to 1 M. After stirring at room temperature for a day, the resulting clear solution was slowly evaporated on a rotary evaporator at 313 K until crystals appeared (about 50% reduction in volume). The mixture was then cooled to 278 K, and its temperature was maintained for a day. The D4R crystals were recovered, carefully dried between filter papers, and subsequently put directly into a Teflon-lined autoclave without adding water. The closed autoclave was heated at 423 K for 7 days without rotation. RUB-15 obtained as white powder was isolated by filtration, thoroughly washed with acetone, and dried at 333 K in a convection oven.

**Acidic Pretreatment and Calcination.** The resultant layered silicate RUB-15 was dispersed in an aqueous solution of formic acid, acetic acid, propionic acid, or butyric acid at a concentration that varied from 1 to 9 M. Typically, 0.1 g of RUB-15 was added to 30 mL of the carboxylic acid solution. The resulting suspensions were stirred at room temperature for a specific time period between 10 s and 3 h. Samples were isolated by filtration, briefly washed with distilled water, and dried in an oven at 333 K for a day. The acid-treated samples were then calcined at 1073 K for 5 h under a dry air atmosphere. All of the calcined products are white; the presence of residual carbon cannot be recognized by the naked eye.

**Characterization.** Powder X-ray diffraction (XRD) patterns were collected on an M03X-HF (Bruker AXS) using Cu K $\alpha$  radiation (40 kV, 30 mA) at a scanning rate of 4°/min over a range 5–45° (2 theta). Thermogravimetric (TG) analyses were performed on a PU 4K (Rigaku) equipped with a mass spectrometer (Anelva M-QA200TS) with a heating rate of 5 K/min using a mixture of 10% O<sub>2</sub> and 90% He as a carrier gas. Solid-state NMR spectra were obtained on a Chemagnetics CMS-300 spectrometer. Silicon-29 magic-angle spinning (MAS) NMR spectra were observed at a resonance frequency of 59.7 MHz with a spinning rate of 5 kHz, a pulse width of 2.0  $\mu$ s, and a recycle delay of

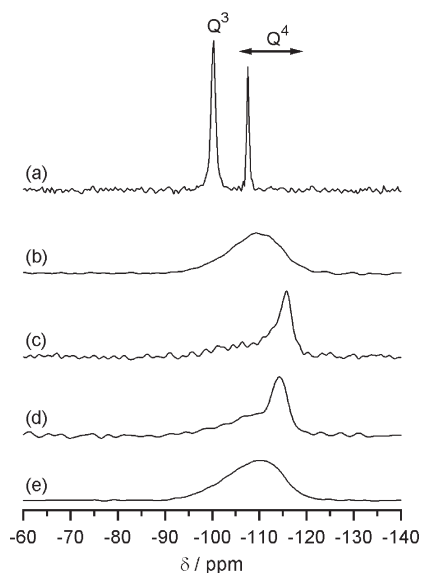


**Figure 2.** Solid-state  $^{29}\text{Si}$  MAS NMR spectra of (a) RUB-15 and those obtained after calcination of RUB-15 treated with (b) 6 M formic acid, (c) 6 M acetic acid, (d) 6 M propionic acid, and (e) 6 M butyric acid for 3 h.

150 s. Carbon-13 cross-polarization (CP)/MAS NMR spectra were recorded at 75.6 MHz with a contact time of 3 ms and a recycle delay of 5 s. Size and morphology of the samples were observed on a field-emission scanning electron microscope (FE-SEM; Hitachi S-4800). Transmission electron microscopic studies were carried out on a JEOL JEM-2010 electron microscope operated at 200 kV. The lamella sample was prepared for TEM by an argon ion milling system (JEOL Ion Slicer, EM-09100IS) after the sheet-like crystals were embedded in an epoxy resin. FT-IR spectra were recorded on a FT-IR spectrometer (JASCO, FT/IR-6100) by the KBr method.

## RESULTS AND DISCUSSION

**Effect of the Type of Carboxylic Acid on the Structure.** The parent layered silicate RUB-15 contains  $\text{TMA}^+$  cations compensating for the negative charges at  $\text{Si}-\text{O}^-$  sites and structured water between the layers.<sup>8</sup> The XRD pattern of RUB-15 shows the strongest peak at  $2\theta = 6.3^\circ$  corresponding to a basal  $d$  spacing of 1.40 nm (Figure S1 of the Supporting Information). Without carboxylic acid treatment, RUB-15 decomposes into amorphous silica upon calcination at 1073 K (Figure S1 of the Supporting Information). Figure 1 shows the powder XRD patterns of RUB-15 treated with varying concentrations of formic, acetic, propionic, or butyric acids ( $\text{C}_n\text{H}_{2n+1}\text{COOH}$ ,  $n = 0, 1, 2,$  and  $3$ , respectively) before and after calcination at 1073 K. As a result of the acid treatment, the basal spacing of RUB-15 decreases to approximately 0.76 nm. This value is close to the thickness of each silicate layer ( $\sim 0.60$  nm), suggesting that  $\text{TMA}^+$  cations and structured water are almost completely removed from the interlayer space of RUB-15. Although the peak positions are similar regardless of the type of carboxylic acid, the peak intensities of the acid-treated samples vary depending on the type and concentration of these acids, leading to a difference in crystallinity of the products after calcination. Under the investigated conditions, well-crystallized sodalite was formed only when acetic or propionic acid in suitable concentrations (3–9 M) was

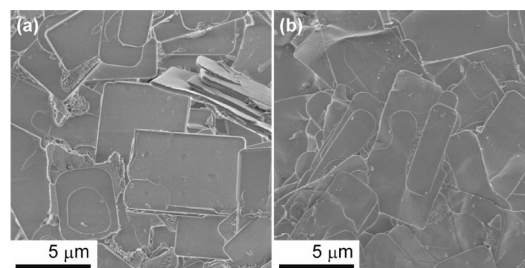


**Figure 3.** FE-SEM images of (a) RUB-15 and (b) sodalite prepared by calcination of RUB-15 treated with 6 M propionic acid for 3 h.

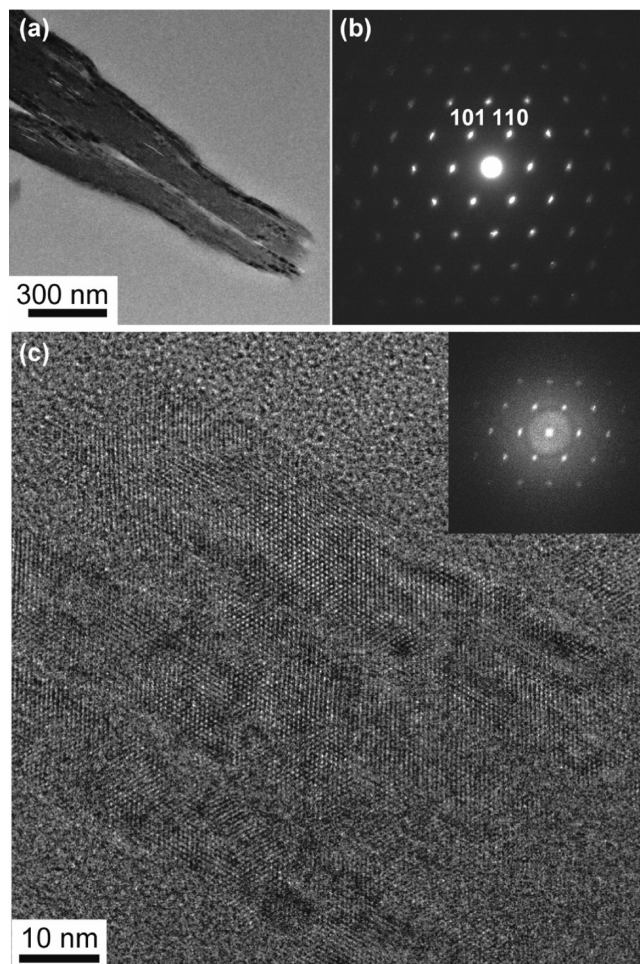


**Figure 4.** Cross-sectional TEM images of sodalite prepared by calcination of RUB-15 treated with 6 M propionic acid for 3 h: (a) low-magnification image, (b) corresponding electron diffraction pattern, and (c) high-resolution image and Fourier diffractogram (inset). Note that the sodalite was very stable under an electron beam; no structural degradation was observed during the observation.

used, while formic or butyric acid treatments led to amorphous or low-crystalline sodalite-like materials after calcination.

Figure 2 shows the solid-state  $^{29}\text{Si}$  MAS NMR spectra of the samples obtained by treatment with carboxylic acids (6 M) followed by calcination. Untreated RUB-15 exhibits two sharp signals corresponding to  $\text{Q}^3$  ( $(\text{SiO})_3\text{SiOH}$  or  $(\text{SiO})_3\text{SiO}^-$ ) and  $\text{Q}^4$  ( $(\text{SiO})_4\text{Si}$ ) sites with the  $\text{Q}^3/\text{Q}^4$  ratio of 2 (Figure 2a).



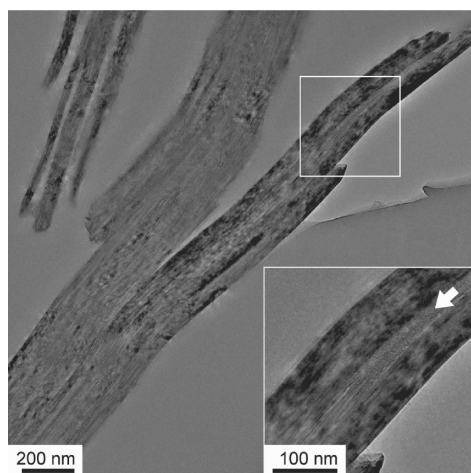


**Figure 5.** Cross-sectional TEM image of sodalite prepared by calcination of RUB-15 treated with 6 M propionic acid for 3 h highlighting the presence of an amorphous region between the crystalline layers.

The  $Q^3/Q^4$  ratio drastically decreased after calcination of the acid-treated samples (Figures 2b–e), indicating that the  $Q^3$  sites were condensed into the  $Q^4$  sites.<sup>7h</sup> The calcined products obtained from the acetic and propionic acid-treated samples show relatively sharp  $Q^4$  signals at  $-115$  ppm, which is ascribed to the crystalline sodalite framework. However, the presence of a relatively small, broad, overlapped signal centered at  $-110$  ppm suggests that amorphous regions are also present in these products. This is consistent with the powder XRD patterns showing broad humps at around  $2\theta = 20\text{--}25^\circ$ , which is a characteristic of amorphous silica. It is noteworthy that only this broad  $Q^4$  signal is observed when samples are treated with either formic or butyric acid, supporting the premise that the resulting Si–O–Si networks are atomically disordered like amorphous silica, which is also consistent with the XRD results. The dehydration condensation of silanol groups was also confirmed by FT-IR (Figure S2 of the Supporting Information). The broad absorption at  $3300\text{ cm}^{-1}$  assigned to O–H stretching vibration of silanol groups on the RUB-15 layer disappeared after calcination (Figure S2 of the Supporting Information).

The product obtained by treatment with 6 M propionic acid for 3 h, which exhibits the most intense and sharpest XRD peaks (Figure 1c), is characterized in detail. As shown in Figure 3, the morphology of this sodalite is rectangle-shaped and sheet-like, similar to the parent RUB-15, suggesting that it was formed in a topotactic manner without decomposition or collapse of the mother silicate layers. Note that this morphology is quite different from those with a cubic symmetry such as rhombic dodecahedral, truncated rhombic dodecahedral, and truncated octahedral morphologies typically observed for conventional sodalite synthesized by hydro-/solvothetical reactions.<sup>10</sup>

Cross-sectional TEM images of the sheet-like particles are shown in Figure 4. The low-magnification image (Figure 4a) shows a partial fissure morphology, and its electron diffraction pattern (Figure 4b) confirms a single-crystalline nature, where the (110) plane of sodalite is parallel to the surface of the sheet.

The high resolution image (Figure 4c) clearly shows that the prepared sodalite is highly crystalline. Careful observation of this sample revealed that, in some parts (indicated by the white arrow in Figure 5), amorphous layers are present between sodalite layers, which is consistent with the XRD and  $^{29}\text{Si}$  MAS NMR

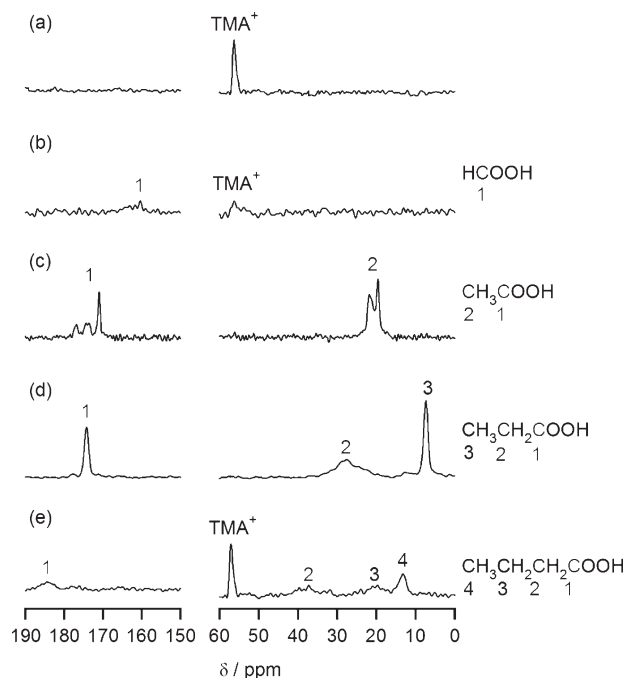


**Figure 6.** Solid-state  $^{13}\text{C}$  CP/MAS NMR spectra of (a) RUB-15 and RUB-15 treated with (b) 6 M formic acid, (c) 6 M acetic acid, (d) 6 M propionic acid, and (e) 6 M butyric acid for 3 h.

results (Figures 1c and 2d). Such amorphous layers are thought to be formed by miss-stacking of silicate layers during dehydration–condensation, though the mechanism is unclear at this time.

Considering that intermediate silicates have a similar interlayer distance, independent of the size of the carboxylic acid employed (Figure 1), one can imply that successful formation of sodalite depends on other essential features such as the amount of interlayer organic species (residual  $\text{TMA}^+$  cations and intercalated carboxylic acid molecules), the presence of a suitable interlayer distance, and the stacking sequence of the intermediate silicates as well as their stability during dehydration–condensation.

Information about interlayer organic species was obtained by solid-state  $^{13}\text{C}$  CP/MAS NMR (Figure 6). The spectra for RUB-15 treated with acetic or propionic acid (6 M) exhibit the signals assigned to acetic acid ( $\delta = 20$  and  $170\text{--}178$  ppm) or propionic acid ( $\delta = 8, 27$ , and  $174$  ppm), respectively (Figures 6c and 6d). These signals are slightly shifted from those observed in the liquid state (data not shown), implying that the carboxylic acid molecules were located between the layers. A signal for the  $\text{TMA}^+$  cations at around  $56$  ppm, which appears in the spectrum of RUB-15 (Figure 6a), is not observed in the spectra of these treated samples, confirming that the  $\text{TMA}^+$  cations are removed from the interlayer space by proton exchange. However, in the cases of formic and butyric acid (Figure 6b and e, respectively), the signals associated with these carboxylic acids are not clearly detected as compared with the samples treated with acetic or propionic acid. In addition, the signal for the  $\text{TMA}^+$  cations remains, confirming that ion exchange has not been completed under identical conditions. It could be expected that such a difference in the interlayer environment is responsible for the difference in the structures of the calcined products.

Considering the crystal structure of RUB-15, it should be noted that neighboring layers need to shift a distance of half the unit cell along the  $c$ -axis to form pure silica sodalite (Scheme 1).

## Scheme 1. Schematic Image of Topotactic Conversion of RUB-15 into Sodalite

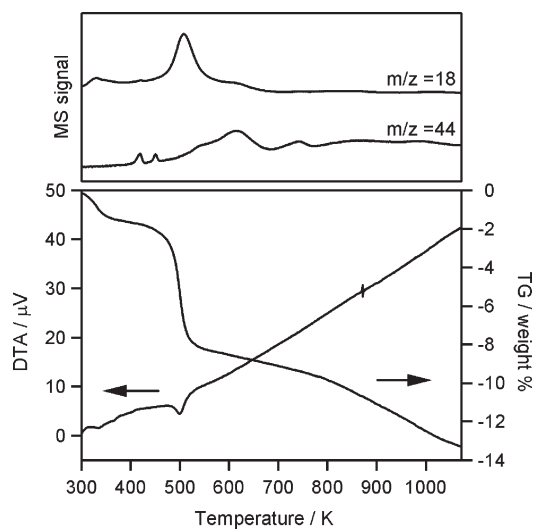
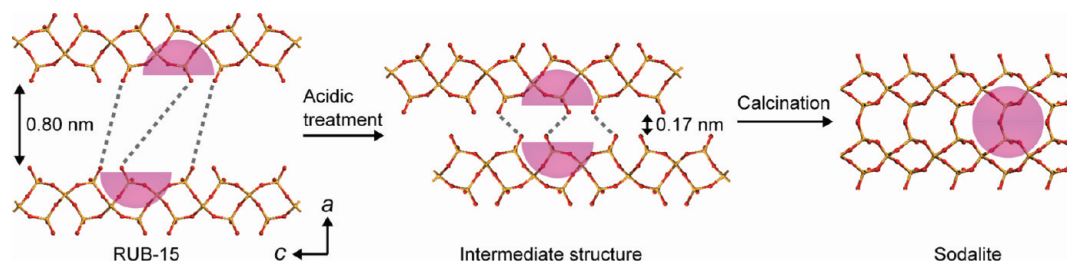


**Figure 7.** TG-DTA curves (bottom) and MS signals (top) of RUB-15 treated with 6 M propionic acid for 3 h.

We speculate that intercalation of the carboxylic acids that can fit over the sodalite half-cups would move the single silicate layers along a direction parallel to the layers ( $bc$  plane; middle of Scheme 1). This is supported by the significant change in electron diffraction patterns obtained when the incident beam is normal to the surface of the sheet-like crystals upon acetic acid treatment (Figure S3 of the Supporting Information).

Also, the small  $d$  spacings of the acid-treated RUB-15 imply that the intercalated carboxylic acids are partly trapped in the half-cups rather than being fully exposed in the layer surface. It is plausible that, because the amount of intercalated acid is relatively small for formic and butyric acids compared with acetic and propionic acids, silicate layers do not undergo lateral shifting and are therefore transformed into amorphous silica by calcination. Interestingly, sodalites obtained from propionic acid-treated RUB-15 exhibit crystallinity higher than those obtained by treatment with acetic acid. This can be attributed to a difference in the local environments of these carboxylic acids between the silicate layers. The  $^{13}\text{C}$  CP/MAS NMR results show that acetic acid molecules are partly esterified with silanol groups as evidenced by the split signals (Figure 6c).<sup>7h</sup> This is in clear contrast to the results for propionic acid-treated samples, which exhibit the single signal and are thus considered to be in a more uniform environment (Figure 6d).

**Thermal Behavior of Propionic Acid-Treated RUB-15.** The calcination step of an acid-treated intermediate involves dehydration–condensation of the interlayer silanol groups and

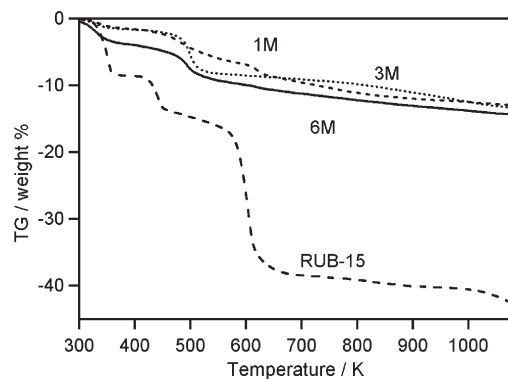


**Figure 8.** TG curves of RUB-15 and RUB-15 treated with various concentrations of propionic acid for 3 h.

decomposition of the intercalated organics. These processes were monitored by TG-MS. Figure 7 shows the TG/DTA-MS curves of RUB-15 after treatment with 6 M propionic acid for 3 h. Below 400 K, a weight loss resulting from desorption of physically adsorbed water is observed. At the higher temperature range of 443–543 K, a steep weight loss ( $\sim 6.2\%$ ) is observed, and water ( $m/z = 18$ ) is detected in the outlet stream. On the basis of our previous results with acetic acid treatment, this weight loss is attributed to condensation of the silanol groups.<sup>7h</sup> The gradual weight loss at higher temperatures (623–1073 K) is accompanied by the generation of  $\text{CO}_2$  ( $m/z = 44$ ) and thus attributed to decomposition of interlayer propionic acid. Note that the window size of the sodalite cage (six-membered ring) allows only very small molecules, for example, He,  $\text{NH}_3$ ,  $\text{H}_2\text{O}$ , and  $\text{H}_2$ , to pass through;<sup>11</sup> therefore, the removal of organic matters occluded in the sodalite cages generally requires collapse or transformation of the cages or both.<sup>12</sup> This fact suggests that, although interlayer condensation proceeds primarily at around 500 K, some uncondensed sites remain until the organic species are completely removed from the interlayer spaces (up to  $\sim 800$  K). The absence of organic residue was also confirmed by FT-IR spectrum (Figure S2 of the Supporting Information), showing no significant absorption other than those of silica was observed after calcination (Figure S2c of the Supporting Information).<sup>9a</sup>

**Effect of the Concentration of Propionic Acid.** As shown in panel (c) of Figure 1, the concentration of propionic acid greatly affects the crystallinity of the intermediate products as well as that of the calcined products. At a concentration of 1 M, only very weak XRD peaks are observed after acid treatment, and the corresponding calcined sample is almost amorphous. This is probably because of a low degree of ion exchange, which leads to

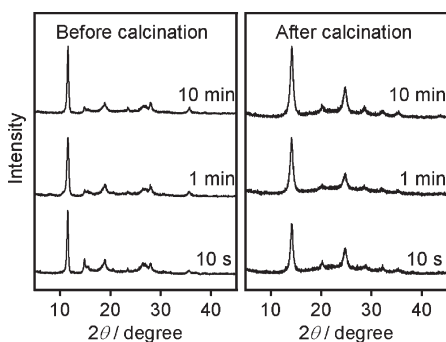


**Figure 9.** XRD patterns of RUB-15 treated with 3 M propionic acid for various time periods: (left) before and (right) after calcination. Note that after stirring, the samples were still immersed in the propionic acid solution for about 20 s during filtration.

a nonuniform interlayer distance. At a concentration of 6 M, the strongest XRD peaks are observed, indicating that the layered structure was well maintained after treatment with the acid. Judging from the XRD patterns, the sodalite obtained by calcination of this intermediate product exhibits the highest crystallinity.

Figure 8 compares the TG curve of RUB-15 with those of the samples treated with different concentrations of propionic acid for 3 h. Untreated RUB-15 shows a total weight loss of approximately 43%, and this value is same as that (42.97%) estimated from its chemical composition ( $[\text{N}(\text{CH}_3)_4]_8[\text{Si}_2\text{O}_5(\text{OH})_4] \cdot 20\text{H}_2\text{O}$ ). Three weight loss steps are observed in the temperature ranges of 323–373 K, 413–453 K, and 563–653 K, and the reductions resulted primarily from removal of adsorbed water, interlayer structured water, and decomposition of  $\text{TMA}^+$  cations, respectively (MS data not shown). The sample treated with 3 M propionic acid, which yields well-crystallized sodalite (Figure 1c), exhibits a TG curve similar to that for the 6 M acid-treated sample, although there is little difference in the amount of physically adsorbed water. In fact, both the presence of propionic acid and the absence of  $\text{TMA}^+$  cations between the layers were confirmed by  $^{13}\text{C}$  CP/MAS NMR (Figure S4 of the Supporting Information).

On the other hand, the sample treated with 1 M propionic acid shows an additional weight loss at approximately 600 K similar to RUB-15. This result suggests that  $\text{TMA}^+$  cations remain in the sample to some degree. In fact, nitrogen oxides ( $\text{NO}$ :  $m/z = 30$ ;  $\text{NO}_2$ :  $m/z = 46$ ) are detected by MS in the wide temperature range of 500–930 K. It is also noteworthy that relatively small and more moderate weight loss steps as well as broader MS signals ( $m/z = 18$ ) due to condensation of silanol groups (443–543 K) are observed (Figure S5 of the Supporting Information). It appears that the presence of  $\text{TMA}^+$  cations after a prolonged treatment reflects poor diffusion and ion-exchange of propionic acid, which leads to poor intermediate structures (Figure 1c) and incomplete condensation of silanol groups, resulting in poor crystallinity of the calcined sample.

**Effect of Treatment Time with Propionic Acid.** We also investigated different parameters as a function of treatment time. The time-dependent variation in pH during acidic treatment of the dispersion with 3 M propionic acid was measured (Figure S6 of the Supporting Information). A pH increase from 1.8 to 2.1 was observed immediately after the addition of RUB-15, and the pH became constant after 1 min. This pH increase is explained by the occurrence of ion-exchange between  $\text{H}^+$  and the interlayer

$\text{TMA}^+$  cations. Considering the sheet-like morphology of RUB-15, such a rapid exchange might be attributed to proton diffusion along the direction normal to the silicate layers (i.e., through a six-membered siloxane ring) in addition to diffusion through the interlayer. It is plausible that  $\text{TMA}^+$  cations are almost completely released from the interlayer within 1 min with coincident formation of  $\text{Si}-\text{OH}$  from  $\text{Si}-\text{O}^-$ . However, even after 10 min, MS analysis of the acid-treated sample detected nitrogen oxides ( $m/z = 30$  and 46) at >480 K (Figure S5 of the Supporting Information), indicating that a portion of the  $\text{TMA}^+$  cations is still present in the interlayer spaces. This is also supported by  $^{13}\text{C}$  CP/MAS NMR (Figure S4 of the Supporting Information).

Figure 9 shows the XRD patterns of the samples treated with propionic acid for 10 s, 1 min, and 10 min before and after calcination. The acid-treated samples exhibit similar ordered intermediate states, but the crystallinity (i.e., intensity of the (110) peak) of the calcined products gradually increases with time, up to 10 min. No further increase is observed after 10 min as there is no difference in the crystallinity of the calcined samples treated for 10 min and those treated for 3 h (Figure 1c), although MS profiles ( $m/z = 18, 30, 44,$  and 46) of these samples are quite different (Figure S5 of the Supporting Information) mainly due to the presence of residual  $\text{TMA}^+$  cations in the 10 min sample. It seems that complete removal of  $\text{TMA}^+$  cations prior to calcination is not a prerequisite for the formation of well-crystallized sodalite. In contrast to the sample treated with 1 M propionic acid for 3 h, we speculate that treatment of RUB-15 with 3 M propionic acid for as short as 10 min (Figure 9, middle) can provide a certain degree of ion-exchange and intercalation. Although  $\text{TMA}^+$  cations were not completely removed, these ions together with intercalated propionic acid molecules could stabilize the intermediate structures. Thus, the concentration of acid would be a key determinant in the formation of these stabilized structures as it can strongly affect molecular diffusion and the resulting number of molecules existing between the silicate layers.

**Key Factors for Topotactic Conversion.** As we reported previously,<sup>7h</sup> only amorphous silica was obtained when RUB-15 was treated with HCl. In this case,  $\text{TMA}^+$  cations are completely exchanged with protons, but the resulting products have poorly crystallized structures possibly due to miss-stacking or distortion of the layers or both in the absence of intercalated organic molecules. However, more recently, Plevert et al.<sup>13</sup> reported that the RUB-15 precursor for topotactic conversion can be obtained by incomplete cation exchange using HCl. From these results and together with our findings described above, it is reasonable to conclude that the exchange of  $\text{TMA}^+$  cations with protons, which decreases the interlayer distances while maintaining the well-ordered layered structure owing to the presence of a small but appropriate amount of interlayer organic molecules such as  $\text{TMA}^+$  cations and carboxylic acids is essential for the conversion of RUB-15 into pure silica sodalite. Compared with HCl, the use of a carboxylic acid is more effective not only because it provides protons for cation exchange but also because it is intercalated between layers thereby maintaining the well-ordered layered structure even after complete removal of the interlayer  $\text{TMA}^+$  cations. To achieve well-crystallized sodalite, pretreatment with a carboxylic acid with suitable structure is required. This is probably because of either a molecular size associated steric effect or a pH-associated inductive effect or a combination of these factors for the acids examined in this study.



## CONCLUSION

The role of acidic pretreatment in topotactic conversion of a layered silicate RUB-15 into pure silica sodalite has been investigated. The type and concentration of carboxylic acid strongly affected the structure of the resulting products. Treatment with propionic acid under suitable conditions resulted in the formation of sodalite with crystallinity higher than that obtained using other carboxylic acids, including acetic acid, which was used previously.<sup>7h</sup> The sodalite prepared in this manner has a unique sheet-like morphology where the (110) plane is parallel to the sheet surface. Two key factors for such successful conversion are found as follows: (i) proton exchange of interlayer TMA<sup>+</sup> cations to shorten the interlayer distance and to form Si–OH groups and (ii) intercalation of carboxylic acid molecules between the layers to maintain the well-ordered layered structure prior to calcination. We believe that these findings would contribute to the topotactic synthesis of other types of zeolite as well.

## ASSOCIATED CONTENT

**S Supporting Information.** XRD patterns, FT-IR spectra, electron diffraction patterns, solid state <sup>13</sup>C CP/MAS NMR spectra, MS spectra, and pH variation. This material is available free of charge via the Internet at <http://pubs.acs.org>.

## AUTHOR INFORMATION

### Corresponding Author

\* E-mail: [okubo@chemsys.t.u-tokyo.ac.jp](mailto:okubo@chemsys.t.u-tokyo.ac.jp).

### Present Addresses

<sup>5</sup>School of Chemical & Biomolecular Engineering, Georgia Institute of Technology, 311 Ferst Drive, Atlanta, GA 30332, USA

## ACKNOWLEDGMENT

This work was supported in part by Grants-in-Aid for Scientific Research (B) and for JSPS Fellows by the Japan Society for the Promotion of Science (JSPS). T.M. is a JSPS research fellow and is grateful to JSPS for Research Fellowships for Young Scientists. Y.S. acknowledges support from SCF (Special Coordination Funds for Promoting Science and Technology) by MEXT of Japan. We thank Dr. Y. Kamimura (The University of Tokyo) for solid-state NMR measurements.

## REFERENCES

- (1) (a) Davis, M. E. *Nature* **2002**, *417*, 813–821. (b) Kitagawa, S.; Kitaura, R.; Noro, S. *Angew. Chem., Int. Ed.* **2004**, *43*, 2334–2375.
- (2) Database of Zeolite Structures. <http://www.iza-structure.org/databases/>.
- (3) (a) de Moor, P. P. E. A.; Beelen, T. P. M.; Komanschek, B. U.; Beck, L. W.; Wagner, P.; Davis, M. E.; van Santen, R. A. *Chem.—Eur. J.* **1999**, *5*, 2083–2088. (b) Davis, T. M.; Drews, T. O.; Ramanan, H.; He, C.; Dong, J. S.; Schnablegger, H.; Katsoulakis, M. A.; Kokkoli, E.; McCormick, A. V.; Penn, R. L.; Tsapatsis, M. *Nat. Mater.* **2006**, *5*, 400–408.
- (4) (a) Davis, M. E.; Lobo, R. F. *Chem. Mater.* **1992**, *4*, 756–768. (b) Lobo, R. F.; Zones, S. I.; Davis, M. E. *J. Inclusion Phenom. Mol. Recognit. Chem.* **1995**, *21*, 47–78. (c) Corma, A.; Davis, M. E. *ChemPhysChem* **2004**, *5*, 304–313.
- (5) (a) Eddaoudi, M.; Moler, D. B.; Li, H. L.; Chen, B. L.; Reineke, T. M.; O’Keeffe, M.; Yaghi, O. M. *Acc. Chem. Res.* **2001**, *34*, 319–330. (b)

Perry, J. J., IV; Perman, J. A.; Zaworotko, M. J. *Chem. Soc. Rev.* **2009**, *38*, 1400–1417.

(6) (a) Rowsell, J. L. C.; Yaghi, O. M. *Angew. Chem., Int. Ed.* **2005**, *44*, 4670–4679. (b) Dincă, M.; Long, J. R. *Angew. Chem., Int. Ed.* **2008**, *47*, 6766–6779. (c) Ma, L.; Abney, C.; Lin, W. *Chem. Soc. Rev.* **2009**, *38*, 1248–1256.

(7) (a) Millini, R.; Perego, G.; Parker, W. O., Jr.; Bellussi, G.; Carluccio, L. *Microporous Mater.* **1995**, *4*, 221–230. (b) Schreyeck, L.; Caullet, P.; Mougénel, J. C.; Guth, J. L.; Marler, B. *Microporous Mater.* **1996**, *6*, 259–271. (c) Ikeda, T.; Akiyama, Y.; Oumi, Y.; Kawai, A.; Mizukami, F. *Angew. Chem., Int. Ed.* **2004**, *43*, 4892–4896. (d) Zanardi, S.; Alberti, A.; Cruciani, G.; Corma, A.; Fornés, V.; Brunelli, M. *Angew. Chem., Int. Ed.* **2004**, *43*, 4933–4973. (e) Marler, B.; Cambor, M. A.; Gies, H. *Microporous Mesoporous Mater.* **2006**, *90*, 87–101. (f) Marler, B.; Ströter, N.; Gies, H. *Microporous Mesoporous Mater.* **2005**, *83*, 201–211. (g) Wang, Y. X.; Gies, H.; Marler, B.; Müller, U. *Chem. Mater.* **2005**, *17*, 43–49. (h) Moteki, T.; Chaikititilp, W.; Shimajima, A.; Okubo, T. *J. Am. Chem. Soc.* **2008**, *130*, 15780–15781.

(8) Oberhagemann, U.; Bayat, P.; Marler, B.; Gies, H.; Rius, J. *Angew. Chem., Int. Ed.* **1996**, *35*, 2869–2872.

(9) (a) Oumi, Y.; Takeoka, T.; Ikeda, T.; Yokoyama, T.; Sano, T. *New J. Chem.* **2007**, *31*, 593–597. (b) Ikeda, T.; Oumi, Y.; Takeoka, T.; Yokoyama, T.; Sano, T.; Hanaoka, T. *Microporous Mesoporous Mater.* **2008**, *110*, 488–500.

(10) Bibby, D. M.; Dale, M. P. *Nature* **1985**, *317*, 157–158.

(11) Breck, D. W. In *Zeolite Molecular Sieves*; Wiley: New York, 1974.

(12) (a) Münzer, S.; Caro, J.; Behrens, P. *Microporous Mesoporous Mater.* **2008**, *110*, 3–10. (b) King, R. S. P.; Dann, S. E.; Elsegood, M. R. J.; Kelly, P. F.; Mortimer, R. J. *Chem.—Eur. J.* **2009**, *15*, 5441–5443.

(13) Plévert, J.; Tatsumi, T. In *Extended Abstracts of the International Symposium on Zeolites and Microporous Materials 2009*, Japan, Abstract No. OC-2-4.

(14) (a) Hasegawa, I.; Kuroda, K.; Kato, C. *Bull. Chem. Soc. Jpn.* **1986**, *59*, 2279–2283. (b) Smolin, Y. I.; Shepelev, Y. F.; Pomes, R.; Hoebbel, D.; Wieker, W. *Sov. Phys. Crystallogr.* **1979**, *24*, 19–23.